Iranian Journal of Fuzzy Systems

Volume 22, Number 6, (2025), pp. 103-123

Original paper

University of Sistan and Baluchestan

An integrated deep learning and fuzzy logic system for road crack severity analysis, and pedestrian fall risk prediction

P. S. Chakurkar [1] and D. Vora [2]

[1,2] *Symbiosis Institute of Technology, PUNE, Symbiosis International (Deemed University), Pune, India*
[1] *School of Computer Engineering, Dr. Vishwanath Karad, MIT WORLD PEACE UNIVERSITY, Kothrud, Pune, Maharashtra, India; 411038*

priti.chakurkar@mitwpu.edu.in, deepali.vora@sitpune.edu.in

Abstract

Cracks on pedestrian sidewalks and walkways pose a significant safety hazard, increasing the risk of trips, falls, and injuries, particularly for vulnerable groups such as the elderly and children. Traditional crack detection and severity assessment methods are usually manual, time-consuming, and subjective, especially in the Indian context, where road and sidewalk inspections are still conducted mainly through visual surveys due to cost and infrastructure constraints. This paper proposes an integrated framework of deep learning and fuzzy logic to analyze sidewalk crack severity and predict pedestrian fall risk automatically. A novel crack quantification method using edge detection and adaptive segmentation is proposed to measure crack width accurately. A fine-tuned deep learning model is employed for automating crack severity prediction, which achieved 95% accuracy and demonstrated robustness to noise, blur, and lighting variations. To estimate fall risk, a fuzzy inference system is developed considering four inputs: crack severity, road condition, weather, and pedestrian age, and a set of expert-defined fuzzy rules is applied to estimate risk levels. The outcomes show the effectiveness of the proposed FIS scheme, which achieved 95% accuracy and outperformed non-fuzzy baseline approaches.

Keywords: Road crack quantification, crack severity, deep learning, pedestrian falling risk, fuzzy logic, triangular membership function.

1 Introduction

Ensuring pedestrian safety is a key issue in urban ecosystems, as adverse road conditions often lead to traffic accidents and the risk of pedestrian injury [8]. Pavement cracks, mainly those found on sidewalks and pedestrian pathways rather than vehicle carriageways, are one of the most common forms of road destruction that can increase the risk of falls, especially for vulnerable age groups such as older people and children. However, the current practices of road inspection are still subject to the random nature of manual inspections, which are a time-consuming, labor-intensive process and prone to human error. Although some developed nations (e.g., the United States, Japan, and several European countries) have widely deployed automated pavement inspection vehicles equipped with high-resolution cameras, lasers, and ground-penetrating sensors, in India and other developing regions, road inspections remain predominantly manual or semi-manual. This is mainly due to the high cost of automated survey machinery, limited availability of specialized infrastructure, and dependencies on municipal staff for visual assessments. As a result, inspections in the Indian context often suffer from incomplete coverage, subjectivity, and inconsistency, highlighting the need for low-cost and automated solutions. In addition, accurate crack quantification, i.e., measuring the width, length, and depth of cracks, is essential for assessing pavement structural deterioration and crack severity. However, this process is also inadequate as manual data collection is slow and often incomplete, as environmental factors and traffic restrict thorough inspections, and

Corresponding Author: D. Vora
Received: July 2025; Revised: September 2025; Accepted: October 2025.
https://doi.org/10.22111/ijfs.2025.52137.9268

only a portion of the sample containing cracks is inspected. Additionally, subjective decisions taken by inspectors in choosing the correct location and crack orientation are often subject to various issues, producing inconsistent data that affects pavement maintenance decisions. Given the expansion of urban infrastructure and changing road conditions due to weather and traffic loads, there is an urgent need to adopt advanced technologies based on image processing, computer vision, and predictive analytics to automate road monitoring and improve the assessment of pavement cracks. The advancements in computer vision, image sensing, and machine learning (ML) have enabled the development of semi-automated and automated methods for crack detection in pavement images [28]. However, the digital image processing (DIP) techniques can be effective; they often require high-quality images and may perform poorly under varying environmental conditions. The traditional ML approaches highly depend on handcrafted feature extraction method, which basically requires a domain expert, and sometimes DIP-based approaches lack adaptability to diverse and complex crack structures [11]. With the recent advancement in deep learning models, the convolutional neural networks (CNNs) have been widely adopted for crack detection, as they automatically learn features and reduce dependence on manual engineering. However, existing CNN-based methods primarily focus on crack segmentation and detection, and relatively few works address automated crack quantification and severity classification. Even in these cases, severity is often treated superficially, without considering complex crack geometries (e.g., intersections, irregular orientations). Moreover, current severity assessment methods, such as mean-width or pixel-based techniques, are sensitive to noise and overlapping edges, leading to inaccuracies. From a pavement management perspective, different cracks, such as longitudinal, transverse, block, and alligator, can have varied implications for structural performance and pedestrian mobility. Yet, research directly linking these defects to pedestrian fall risks remains scarce [9]. The existing pedestrian safety studies have focused more on medical or traffic-related incidents, with limited exploration of how sidewalk deterioration directly contributes to falls. However, the location of pedestrian citefalls considered in this work refers to sidewalks, crosswalks, and pedestrian zones, not vehicular carriageways. Therefore, this paper presents an integrated framework for crack severity detection and pedestrian fall risk prediction. Firstly, the proposed system performs crack width quantification from road images, and then it uses a deep learning model to classify severity (low, medium, high) based on the measured width. Finally, a fuzzy logic model is implemented to predict the pedestrian fall risk by integrating crack severity, weather, surface conditions, and pedestrian age. Although these research topics could be studied separately, this work integrates them into a combined computational framework, where the crack quantification and severity outputs serve as inputs to a fuzzy inference-based fall risk model. The proposed integration represents the novelty of our study, as it covers both technical crack analysis and practical safety risk assessment for urban pedestrians. The main contributions of this work are highlighted as follows:

- Developing a multi-level crack segmentation scheme using image processing algorithms to accurately measure crack widths, with reduced sensitivity to local irregularities in the crack structure.
- Implementing an efficient CNN model that automates crack severity classification based on the quantified width, supported by constructing a comprehensive image dataset.
- Integrating a fuzzy inference system to predict pedestrian fall risks by considering multiple environmental factors and an expert-driven custom rule base.
- Conducting extensive experimental analysis to validate the effectiveness of the proposed integrated framework for road maintenance and pedestrian safety.

The remainder of this paper is organized as follows. Section 2 reviews related work in crack detection, severity analysis, and risk prediction. Section 3 details the methodology, including the image processing techniques, deep learning model architecture, and fuzzy logic framework. Section 4 presents experimental results and evaluates the performance of the proposed system. Finally, Section 5 concludes the paper by summarizing the key contributions and discussing future research directions.

2 Related work

Image-based road crack detection has been extensively studied in the literature, with a variety of approaches developed for segmentation and classification of cracks. However, accurate estimation of road crack severity is very important in the context of pavement management systems due to their significant impact on pedestrian safety and infrastructure maintenance. Current severity-level assessment approaches heavily depend on crack quantification tasks such as measuring crack length and width. The work by Oliveira et al. [19] calculated the average crack width by comparing the pixel count of the entire crack area to its central skeleton. However, this approach is only effective for cracks with a

uniform width, which is not always the case in real-world scenarios where road cracks are subject to significant variations in width along their length. Similar work can be seen by Song et al. [25], where a CNN with a multi-scale attention network is used to classify cracks as transversal, longitudinal, block, or alligator. Further, severity levels such as heavy and light cracks are assessed by computing the average width of crack pixels. Liu et al. [20] improved measurement direction via orthogonal projection, increasing accuracy, but their method is sensitive to intersecting artifacts.

There are also a few research studies exploring fuzzy logic methods for handling uncertainty in crack classification and pavement assessment. The work by Hussain and Alam [12] incorporated fuzzy logic with neural networks using Gaussian membership functions to improve road crack detection and classification. Similarly, Ranjbar et al. [22] integrated fuzzy logic with metaheuristic optimization algorithms to improve the severity analysis of pavement distress. Another work by Mathavan et al. [18] introduced a fuzzy Hough transform to detect low-contrast pavement cracks in images. Ali et al. [2] utilized fuzzy logic to address uncertainty in pavement distress evaluation to compute the Pavement Condition Index (PCI). However, as noted in Karaşahin and Terzi [14], most fuzzy models focus on deterioration prediction rather than real-time severity assessment. Saeed et al. [24] predicted road deterioration in asphalt surfaces using applied fuzzy logic, but did not focus on crack severity. It has been observed that there is limited research on integrating fuzzy logic with real-time road crack quantification and pedestrian safety risk analysis, as most of the studies have been subjected to pavement management systems and structural deterioration analysis.

In terms of deep learning, Yang et al. [29] used a fully convolutional network for pixel-level segmentation and crack width and length quantification, but achieved slightly lower accuracy. In a similar direction, Yuan et al. [31] designed a ResNet-50 based model with feature pyramid and attention layers to increase segmentation accuracy. Ali et al. [1] enhanced segmentation using a residual U-Net with constrained blocks and sharpening filters, classifying severity using morphology. Deng et al. [6] combined YOLOv5 with pixel segmentation to improve accuracy in challenging conditions. The work by Chakurkar et al. [4] presented a contextual U-Net-based model with hierarchical attention for performing crack segmentation against varying environmental conditions. Ha et al. [10] presented a multi-CNN framework for max-width-based severity analysis. Though this model achieved good accuracy, it required higher computational complexity. Kumar and Tung [15] proposed a YOLOv8-based framework for detecting potholes and multiple crack types, integrating severity assessment with high accuracy, though limited to bounding-box detection.

Post-disaster applications have also emerged; Yilmaz et al. [30] developed a deep learning–based segmentation system for earthquake-induced cracks, creating a unique dataset but remaining context-specific. Optimized CNN approaches have also shown strong performance. Elghaish et al. [7] introduced a multi-layer CNN with feature selection, achieving F-scores above 98%, though requiring high computational resources and large datasets. Similarly, Demir et al. [5] proposed CrackNet, combining ConvMixer and ReliefF-SVM to classify major and minor cracks, reports 94.2% accuracy but offering limited granularity. Segmentation-based models have also been refined. Wang et al. [27] proposed a Depth-Supervision FRRN to address vanishing gradients, improving crack delineation over standard FRRN. In contrast, unsupervised approaches remain attractive where labeled data is scarce. Bhardwaj et al. [3] presented a fuzzy C-means clustering method effective in noisy or low-contrast conditions, though it lacks higher-level severity assessment.

However, it can be seen that the deep learning approaches mainly targeted crack segmentation but not automated severity classification. Also, fuzzy logic-based approaches are primarily subjected to pavement distress evaluation, but their direct application in road crack severity and pedestrian risk prediction remains unexplored. Pedestrian fall risk prediction based on quantified crack severity remains largely unexplored. Hence, a clear gap exists in that no universally accepted framework has been reported for categorizing crack severity levels based on quantified crack attributes. There is a need to introduce a computationally efficient framework for real-time applications that can handle complex road crack images without sacrificing accuracy.

3 Methodology

The proposed framework aims to provide an integrated and automated system for road crack severity classification and pedestrian fall risk prediction that can serve as a proactive decision-support tool for urban infrastructure safety. The system includes three main phases: (i) crack quantification, (ii) severity analysis, and (iii) pedestrian fall risk estimation (see Figure 1). The binary road crack images are processed as input images to generate a confidence map via edge detection. Then, an adaptive segmentation approach is proposed to identify and quantify crack regions, followed by skeletonization, intersection point detection, and distance transform to extract maximum crack widths per segment. These quantified widths are annotated by predefined severity thresholds (high, medium, low), creating a labeled dataset to train a deep CNN (EfficientNetB0) for severity prediction. Predicted severity and contextual factors (e.g., weather, pedestrian demographics) are fed into a Mamdani-type fuzzy inference system, which computes real-time fall risk rates using expert-defined rules. This multi-level approach supports deployment on diverse surfaces and

prioritizes maintenance in high-risk, vulnerable zones. The novelty of the proposed system is its integrated approach, which combines edge-based crack detection, adaptive segmentation, deep learning-driven severity classification, and fuzzy logic-based fall risk prediction for proactive pedestrian safety.

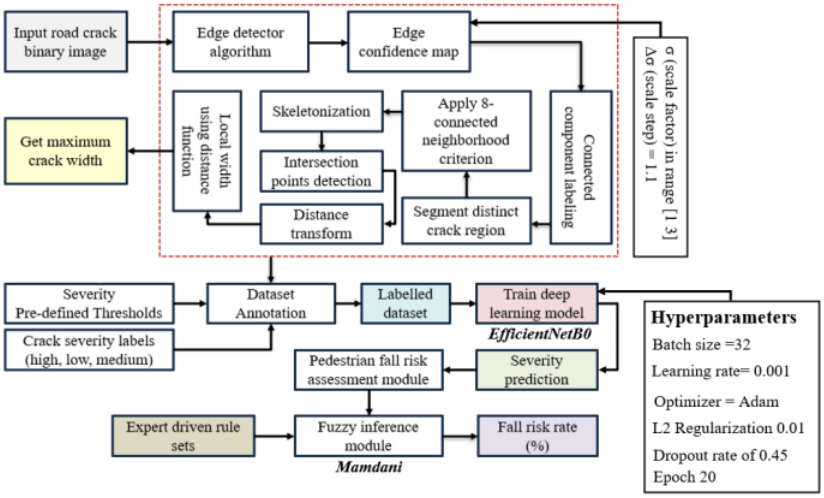

Figure 1: Illustrate the Schematic Architecture of the Proposed System

3.1 Crack quantification

The proposed study presents a lightweight and effective crack quantification method that addresses the problems of over- or underestimation in width measurement, which typically arise from assuming uniform width along the crack path or relying on perpendicular projections from a central skeleton. Such simplifications fail to capture real-world cracks that frequently exhibit irregular, varying widths, and intersections.

The proposed study considers the crack region as $\Omega \subset \mathbb{R}^2$, where each point in Ω represents part of the crack path on the road surface. Therefore, the objective function F is defined to quantify the accuracy of width measurement by minimizing deviations from true edge distances, such that:

$$F = \sum_{k=1}^{m} \sum_{j=1}^{m_k} \left(w_{(k,j)} - \hat{w}_{(k,j)} \right)^2 . \tag{1}$$

Where $w_{(k,j)}$ represents the computed crack width, closely approximating the actual width $\hat{w}_{(k,j)}$, at point $p_{(k,j)}$ and m_k is the number of points in segment S_k. In this regard, the study aims to minimize F such that the predicted, width $w_{(k,j)}$ aligns as closely as possible with the actual crack width at all segments and points, thereby obtaining an accurate and reliable quantification of the crack severity.

3.1.1 Edge detector algorithm

Crack lines in road surface images are often thin, weakly connected, and highly variable in orientation and width. To better detect and enhance these complex structures, this study introduces an edge detector algorithm utilizing the Hessian matrix and second-order derivatives for enhanced sensitivity to elongated, line-like features. The algorithm, detailed in Algorithm 1, generates a multi-scale edge confidence map that adapts to local variations in crack width and directionality, while retaining both intensity and directional information within the image. The proposed algorithm takes a binary image as input and uses parameters scale factor $\sigma \in [1, 3]$ and scale step $\Delta\sigma = 1.1$, allowing adaptability to local width variations. The eigenvalues obtained from the Hessian matrix capture both intensity and directional information, identifying the primary direction and crack structure. This enhances edge detection even for cracks that change direction, intersect, or exhibit irregular boundaries. The algorithm preserves crack continuity and reduces noise from abrupt directional shifts. The final edge confidence map is produced by selecting maximum responses across scales and normalizing to improve contrast, thereby supporting enhanced crack visibility for subsequent segmentation and quantification.

The proposed multi-scale, orientation-sensitive algorithm addresses three issues in binary crack quantification that standard morphological operations cannot resolve alone:

- **Width-Adaptive Detection:** Multi-scale σ enables adaptability to local width variations, unlike morphological operations that need manually tuned kernels, which may miss thin cracks or overly smooth wider ones.
- **Directional Agnosticism:** Hessian eigenvalues ensure sensitivity to principal curvatures, and enhance crack-like structures regardless of orientation while morphological gradients are biased toward predefined axes.
- **Topological Preservation:** The Hessian-based edge confidence map maintains connectivity at intersections and branching points(see Figure 2 (b)).

Although minor artifacts may remain in weakly connected regions, the post-processing using morphological closing and opening operations ensures structural integrity, which produces suitable output for reliable crack severity and fall risk analysis.

Algorithm 1 Edge confidence map computation

Input: I (Input binary image), σ (Scaling factor), $\Delta\sigma$ (Scale step)
Output: E (Edge confidence map)

Initialize $E(x, y) = 0 \; \forall \; (x, y)$ to store maximum response at each pixel
for each scaling factor σ in range $[\sigma_{\min}, \sigma_{\max}]$ with increments of $\Delta\sigma$ **do**
    Convolve I with Gaussian kernel $G_\sigma(x, y)$ to perform smoothing:

$$I_\sigma(x, y) = G_\sigma(x, y) * I(x, y), \quad \text{where} \quad G_\sigma(x, y) = \frac{1}{2\pi\sigma^2} \exp\left(-\frac{x^2 + y^2}{2\sigma^2}\right)$$

    Compute second-order Gaussian derivatives of I_σ to construct Hessian matrix $H_\sigma(x, y)$:

$$H_\sigma(x, y) = \begin{bmatrix} \frac{\partial^2 I_\sigma}{\partial x^2} & \frac{\partial^2 I_\sigma}{\partial x \partial y} \\ \frac{\partial^2 I_\sigma}{\partial y \partial x} & \frac{\partial^2 I_\sigma}{\partial y^2} \end{bmatrix}$$

    for each pixel (x, y) **do**
        Compute eigenvalues λ_1 and λ_2 of $H_\sigma(x, y)$, where $|\lambda_1| \geq |\lambda_2|$
        Compute the edge response:

$$R_\sigma(x, y) = |\lambda_1| \times \exp\left(-\frac{|\lambda_2|}{\sigma^2}\right)$$

        ▷ $R_\sigma(x, y)$ is sensitive to line-structures due to influence of λ_1
        Update edge confidence map:

$$E(x, y) = \max(E(x, y), R_\sigma(x, y))$$

    end for
end for
Normalize E for contrast enhancement:

$$E(x, y) = \frac{E(x, y) - \min(E)}{\max(E) - \min(E)}$$

3.1.2 Adaptive segmentation

Unlike previous methods focused solely on segmenting connected components, this study introduces an adaptive segmentation process that considers orientation changes and reduces measurement direction dependency. The segmentation proceeds in two steps: (i) primary segmentation and (ii) secondary segmentation. The primary segmentation is introduced to identify unique crack regions from $I_{\text{bin}} \in \{0, 1\}^{M \times N}$ using labeling function $L : \mathbb{Z}^2 \to \mathbb{Z}$, which is defined to assign a unique integer label to each connected component in the binary image, such that:

$$L(x, y) = k, \quad \forall (x, y) \in \Omega_k, \tag{2}$$

where $\Omega_k \subset \mathbb{R}^2$ denotes the set of all pixels belonging to the k-th connected component, and N is the total connected components detected. The proposed approach adopts an 8-connected neighborhood criterion to determine adjacency, such that: pixel (x, y) is considered connected to any neighboring pixel $(x+i, y+j)$, for $i, j \in \{-1, 0, 1\}$, and it excludes if $(i, j) = (0, 0)$. Another function $C(\cdot)$ is defined, which operates on I_{bin} by iteratively grouping pixels into distinct sets Ω_k based on this neighborhood connectivity to generate a labelled image $L \in \mathbb{Z}^{M \times N}$ as given in Equ (3).

$$L(x, y) = C(I_{\text{bin}}(x, y)). \tag{3}$$

Therefore, the output image $L(x, y)$ maintains the same size as I_{bin}, where each labeled region, corresponding to a connected component, is assigned a unique identifier $k \in \{1, 2, 3, \cdots, N\}$ with $N = \text{card}(\{k \mid \Omega_k \neq \emptyset\})$ being the total number of identified crack regions. Each region is then analyzed independently for crack attributes (width, length, orientation), minimizing interference. The spatial extent of each segment Ω_k is computed as given in Equ (4):

$$S_k = \sum_{(x,y)\in\Omega_k} I_{\text{bin}}(x, y). \tag{4}$$

Where S_k is a measure of the spatial extent of each crack segment, which is then sorted in descending order to prioritize the analysis of more prominent crack regions. Secondary segmentation addresses complex cracks with intersections, branches, or orientation changes by further dividing regions along curvature and intersections. In this process, the obtained region Ω_k initially undergoes a skeletonization process to obtain a single-pixel-wide medial axis $S_k \subset \Omega_k$, where each skeleton pixel represents the central path of the crack. This simplified operation basically supports localized geometric analysis and intersection detection. The algorithm then detects intersection points $I_p(x, y)$ along the skeletonized crack line by examining each pixel's neighborhood in the skeleton and marking locations considering that three or more neighboring pixels are part of the skeleton, given as Equ (5):

$$I_p(x, y) = \sum_{\text{neighbors}} S_k(x_i, y_i) \geq 3. \tag{5}$$

Therefore, by computing the intersection point the, algorithm effectively isolates continuous crack segments within each primary region that is further labeled individually, such that: $\{\Gamma_{(k,i)}\}_{i=1}^{m_k}$, where $\Gamma_{(k,i)}$ denotes the i-th segment of the k-th primary region and m_k is the total number of segments within that region. A sample visualization of the crack segments separated by secondary segmentation is shown in Figure 2 (a). The core significance of the proposed crack quantification is isolating crack sub-segments at intersections and high-curvature points (see Eq. 6), so each segment $\Gamma_{(k,i)}$ becomes quasi-linear and satisfies the assumption of parallel or near-parallel crack edges. Within each segment, the minimal value of the distance transform at a skeleton pixel gives the true orthogonal width to the local boundary (see Eq. 7), eliminating the need for explicit tangent or normal estimation. This segmentation-based approach improves over traditional single-curve or whole-crack width analysis by:

- Breaking the analysis at intersection and branch points, avoiding width overestimation in these regions;
- Isolating quasi-linear crack segments, for which the EDT assumption is valid and robust; and
- Reducing curvature-induced measurement errors through localized, segment-wise analysis.

3.1.3 Width computation

In this study, maximum crack width is used as the main severity metric instead of average width, based on two observations: (i) average width often misses localized severity due to smoothing over irregular shapes, and (ii) maximum width better indicates structural degradation, as wider cracks usually mean more severe damage [15]. Hence, identifying the maximum segment width is quite important for assessing structural integrity. The algorithm analyzes each segmented region $\Gamma_{(k,i)}$ and calculates a distance transformation $D_k(x, y)$ using the Euclidean distance formula to the nearest boundary pixel $(x', y') \in \delta\Omega_k$, expressed as in Equ (6).

$$D_k(x, y) = \min_{(x',y')\in\delta\Omega_k} \sqrt{(x - x')^2 + (y - y')^2}. \tag{6}$$

Where, $\delta\Omega_k$ denotes the boundary of Ω_k. These localized crack widths are determined by doubling the distance value at each skeleton point $(x, y) \in \Gamma_{(k,i)}$, given as Equ (7):

$$W_k(x, y) = 2 \times D_k(x, y) \quad \forall (x, y) \in R_k. \tag{7}$$

Once the maximum widths are computed for all the segments, they are sorted to find the largest and second-largest widths. The region with the maximum width is identified as the primary region highlighted (red) and second-largest width is also highlighted (orange) for comparative severity analysis as shown in Figure 2 (b).

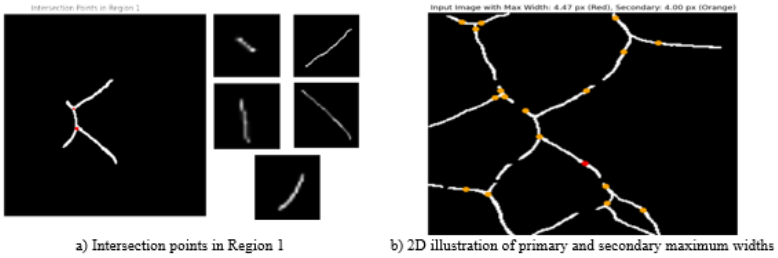

Figure 2: Visualization of intersection points in crack region and quantified maximum width

3.2 Crack severity evaluation and data labeling for automated analysis

This section outlines the process for assessing crack severity based on maximum width and annotating data for automated severity prediction using deep learning. Crack severity is categorized as low, medium, or high. A custom dataset was created by collecting binary road crack images from several public sources (Table 1), ensuring representation across severity levels. The images vary in resolution, lighting, noise, and crack visibility. To standardize inputs, all images were resized to 224×224 pixels, and contrast normalization was applied to improve visibility. A no-crack category was added to address class imbalance and improve the distinction between cracked and non-cracked surfaces. Table 1 summarizes the datasets and image counts. The severity is evaluated using maximum crack width in pixels, as resolution metadata is often unavailable. Following the classification in [10], cracks wider than 10 pixels are labeled high severity (requiring repair), 5–10 pixels as medium, and 0–5 pixels as low or hairline cracks (not requiring immediate repair). These criteria were empirically validated and are summarized as Equ (8):

$$S(W_k) = \begin{cases} \text{Low} & \text{if } W_k < 5 \\ \text{Medium} & \text{if } 5 \leq W_k \leq 10 \\ \text{High} & \text{if } W_k > 10 \\ \text{No\_crack} & \text{if no crack component is detected} \end{cases} \tag{8}$$

The dataset is labeled based on the above criteria mentioned in Equ (8), and then it is split into three subsets: training, validation, and testing, following the split ratio 70%, 15%, and 15%, respectively.

Table 1: Details of the existing dataset used to construct the custom dataset in the proposed work

Ref	êxtbfDataset Name	**Number of Image Samples**
[30]	CFD	118
[7]	CRACK500	2500
[5]	DeepCrack	537
[27]	Ceramic-cracks-dataset	100
[3]	SDNet2018-concrete crack dataset	800

3.3 Deep learning for crack severity prediction

This section presents the methodology for developing a deep learning model to predict crack severity levels from road crack images. EfficientNetB0 CNN architecture was selected for its proven efficiency and robust performance in image classification tasks. Developed by Google in 2019, EfficientNetB0 combines compound scaling, mobile inverted bottleneck convolution (MBConv), and depthwise separable convolutions to balance accuracy and computational efficiency. In this work, EfficientNetB0 is fine-tuned as a feature extractor, initialized with pre-trained ImageNet weights (frozen during initial training). The custom classification layers are added and trained on the labeled crack severity dataset,

allowing the model to learn crack-specific features while avoiding overfitting. The final model includes batch normalization, a dense layer (256 neurons), dropout (0.45), and a 4-neuron output layer for severity classes (low, medium, high, no crack).

3.3.1 Hyperparameters

The training process of the model is optimized through iterative tuning using a grid search technique and validation-based hyperparameter adjustments. The input images are resized to 224×224 pixels for optimal EfficientNet performance. A batch size of 16 balances GPU memory and training stability. The initial learning rate is 0.001, with an adaptive scheduler reducing it if validation loss stagnates. L2 regularization (0.01) is applied to dense weights, L1 activity regularization (0.006) encourages activation sparsity, and dropout (0.45) prevents overfitting. Training was conducted for 20 epochs, as validation accuracy plateaued beyond this point. Data augmentation (random rotation, shifting, flipping) further improves robustness to environmental variations and crack morphology.

3.4 Fuzzy system for pedestrian fall risk analysis

This section presents a computational framework for estimating pedestrian fall risk resulting from road surface irregularities. Though our previous section focused on the automated detection and severity classification of cracks, the current modelling approach extends that work by integrating additional contextual factors such as environmental (e.g., weather, road slipperiness) and demographic (age of the pedestrian) to assess the likelihood of pedestrian falls more comprehensively. The proposed system presents a fuzzy inference mechanism (FIS) to simulate and predict risk under diverse real-world scenarios, where crisp thresholds are inadequate and human reasoning under uncertainty is required.

3.4.1 Motivation and problem statement

In the domain of pedestrian safety, most existing studies mainly emphasized medical conditions or vehicle-related incidents, and neglected the risks associated with deteriorating walking surfaces. Furthermore, those that address infrastructure-related falls either ignore road surface defects or treat them in isolation, and often do not take into account other important contributing factors such as weather effects, surface traction, or pedestrian vulnerability (age-related frailty). Moreover, traditional safety strategies are reactive, where the decision-making process depends on complaints or post-incident data, which limits timely interventions and may ignore emerging hazards in vulnerable areas. To address this issue, the proposed model adopts a proactive risk assessment strategy that supports early warnings for high-risk situations, identification of critical pedestrian areas based on combined risk factors, and data-informed resource allocation for timely maintenance and risk mitigation. The proposed model serves as a decision support system to help city planners, infrastructure maintenance teams, and public health officials prioritize interventions, not only based on the severity of cracks, but also considering who is most at risk, under what circumstances, and where intervention is most critical. Thus, the motivation behind this modeling approach is to transform crack severity analysis into a human-centered, interpretable, and actionable safety framework that guides preventive interventions in complex pedestrian environments.

3.4.2 Modelling approach

Urban pedestrian environments are often subject to complex and ever-changing scenarios, and risk conditions change rapidly. However, a significant problem in developing the pedestrian fall risk model proposed in this study is the lack of a standard experimental dataset to present fall scenarios caused by road defects, weather, and demographic factors. Therefore, the system proposed in this study adopts a Mamdani-type FIS because it can handle uncertainty and imprecision and is well-suited for modeling complex fuzzy inputs. This fuzzy inference-based approach does not require large-scale training data and can integrate expert knowledge for safety-critical applications where interpretability and reliability are essential. To ensure practical relevance and domain validity, the proposed fuzzy modelling approach adopts the following strategies:

- Literature-based variable definitions: The input and output variables and their linguistic categories were derived based on the analysis of previous studies on pedestrian safety, fall risk perception, and infrastructure-related accident research [26]. While factors such as pedestrian familiarity with the route, gender, walking alone vs. accompanied, and body characteristics (height, weight, mobility impairments) have been identified in prior studies as relevant to fall risk [13], they were excluded from this initial framework due to the lack of structured datasets capturing these attributes in the Indian context, as well as the need to maintain a computationally lightweight

and interpretable model. Instead, we focused on four high-impact and data-accessible predictors (crack severity, weather, road surface condition, and pedestrian age), which are consistently cited as critical determinants of fall risk and can be feasibly collected in real-world monitoring systems.

- Rule generation based on real-world analogies: The custom rules are generated considering real-world scenarios (for example, elderly pedestrians walking on foggy, slippery roads are at higher risk) to ensure consistency with existing human factors theory.
- Expert knowledge integration: Three domain experts were consulted to strengthen the reliability of variable selection and rule design. These included one senior traffic engineer, a pavement management specialist, and a researcher in computational intelligence, each with more than ten years of professional or academic experience. They were selected based on their publication record and prior involvement in pedestrian safety projects. Their role was to validate the chosen input variables, refine linguistic terms, and review the completeness and realism of the rule base.

To avoid arbitrary mappings, the study developed a scoring mechanism that gives higher weight to variables with greater impact (e.g., age generally has a larger effect than weather in mild conditions). Multiple experts reviewed these rules to ensure realism, consistency, and effectiveness in capturing pedestrian fall risk. The upcoming section discusses the implementation strategy adopted in the proposed fuzzy-based pedestrian fall risk analysis.

3.4.3 Fuzzy variables

The proposed fuzzy inference system models pedestrian fall risk by capturing the complex interaction between infrastructure defects, environmental hazards, and individual susceptibility [23]. The crack severity index (low, medium, and high) developed in the previous section provides a localized and fine-grained assessment of pavement deterioration, specifically targeting longitudinal and transverse cracks, the most common crack types observed on Indian sidewalks and urban walkways. Although different crack types (e.g., block, alligator) may indeed have varying impacts on pedestrian mobility, this study focuses on longitudinal and transverse cracks due to their higher prevalence and direct influence on tripping hazards in pedestrian zones. Regarding severity scoring, the Pavement Condition Index (PCI) is a widely accepted metric in pavement management, where multiple crack types and distress features are combined into a 0–100 scale for network-level maintenance. However, for pedestrian fall risk modeling, PCI is less suited because it aggregates over large areas and dilutes localized hazards. Therefore, this study adopts a simplified 0–10 crack severity scale, which is directly derived from measured crack width quantification (Section 3.3) and is more interpretable for site-specific pedestrian risk assessment. To capture multi-factor scenarios, the proposed system incorporates multidimensional fuzzy variables, illustrated in Table 2. The system considers a set of four input variables and two output variables, defined mathematically as Equ (9).

$$\mathbf{x} = \left[x_1, x_2, x_3, x_4\right]^T, \quad \mathbf{y} = \left[y_1, y_2\right]^T, \tag{9}$$

where each variable $x_i \in U_{x_i} \subseteq \mathbb{R}$ is defined over a universe of discourse U_{x_i}, divided into fuzzy subsets corresponding to linguistic categories. Therefore, for each variable x_i, a finite fuzzy set is defined in Equ (10):

$$F_{x_i} = \left\{A_i^{(1)}, A_i^{(2)}, \cdots, A_i^{(K_i)}\right\}, \quad \mu_{A_i^{(k)}} : U_{x_i} \to [0,1], \tag{10}$$

where each $A_i^{(k)} \subseteq U_{x_i}$ denotes a fuzzy subset associated with the k^{th} linguistic term (Low, Medium, High) and $\mu_{A_i^{(k)}}$ represents the degree of membership.

Similarly, for each output variable $y_j \in U_{y_j}$ defined over the interval $[0, 100]$, the output fuzzification is given by Equ (11):

$$F_{y_j} = \left\{B_j^{(1)}, B_j^{(2)}, \cdots, B_j^{(M_j)}\right\}, \quad \mu_{B_j^{(k)}} : U_{y_j} \to [0,1]. \tag{11}$$

Here, in Equation (11), each output fuzzy set $B_j^{(k)} \in F_{y_j}$ is associated with a membership function $\mu_{B_j^{(k)}}(y_j)$ which enables the computation of both defuzzified crisp outputs and linguistic interpretations. Table 2 lists the fuzzy variables, their linguistic terms, numerical ranges, membership function (MF) parameters, and rationale. The input variables x_1 through x_3 are normalized to the range $[0, 10]$ using a linear mapping function, and the variable x_4 is retained in its original domain for semantic clarity. The two output variables y_1 and y_2, both defined over $[0, 100]$, basically serve a complementary role, where y_1 provides a qualitative assessment using five linguistic categories, and y_2 offers a quantitative estimate to support decisions such as resource allocation.

Table 2: Fuzzy input and output variables with linguistic terms, numerical ranges, and rationale

		Fuzzy Variables	**Linguistic Terms**	**Range**	**Rationale**
Input	x_1	Crack Severity	F_{x_1} (Low, Medium, High)	0 to 100	Represents physical degradation; higher severity increases tripping risk
	x_2	Weather Conditions	F_{x_2} (Clear, Foggy)	0 to 100	Poor visibility reduces hazard detection capability
	x_3	Road Condition	F_{x_3} (Dry, Wet, Slippery)	0 to 100	Surface traction directly affects fall potential
	x_4	Pedestrian Age	F_{x_4} (Child, Young, Elderly)	0 to 100	Age influences mobility and attentiveness, affecting fall vulnerability
Output	y_1	Fall Risk Level	Very Low, Low, Medium, High, Very High	0 to 100	Provides interpretable, qualitative risk categorization
	y_2	Fall Risk Level	1%, 5%, 20%, 50%, 80%	0 to 100	Offers a quantifiable measure of fall likelihood for decision-making

Table 2 outlines the fuzzy variables used in the system, which serve as the basis for membership function design in the fuzzification module. The input variables x_1 through x_3 are normalized to the range [0, 10] using a linear mapping function, while the variable x_4 is retained in its natural domain for semantic clarity. The two output variables, y_1 and y_2, are not duplicates but complementary, where y_1 provides a qualitative linguistic risk category and y_2 expresses a numerical probability useful for prioritizing interventions and resource allocation. This dual representation improves interpretability for practitioners and supports quantitative analysis in decision-support systems.

3.4.4 Fuzzification process

The fuzzification process is the initial stage of a fuzzy inference system, where crisp numerical inputs are transformed into fuzzy degrees of membership using predefined linguistic terms and membership functions. In the proposed system, fuzzification is applied to each input $x_i \in x$ and output $y_i \in y$ by evaluating their membership in corresponding fuzzy sets.

All fuzzy sets in this study are modeled using triangular membership functions (TriMFs), primarily due to their computational simplicity, intuitive interpretability, and efficiency in rule-based reasoning. Unlike Gaussian or trapezoidal membership functions, which require additional parameters and introduce higher computational overhead, TriMFs allow direct and transparent mappings between linguistic labels and numerical domains, which is essential for safety-critical, real-time pedestrian risk applications.

Also, each TriMF is defined by three parameters (a, b, c), where $a < b < c$ denotes the left foot, peak, and right foot of the triangle, respectively. The TriMFs are numerically represented as follows in Equation (12):

$$\mu(x; a, b, c) = \begin{cases} 0 & \text{if } x \leq a \text{ or } x \geq c \\ \frac{x-a}{b-a} & \text{if } a < x \leq b \\ \frac{c-x}{c-b} & \text{if } b < x < c \end{cases} \tag{12}$$

Here, x denotes a crisp input or output value and $\mu(x; a, b, c) \in [0, 1]$ denotes the corresponding degree of membership in the fuzzy set defined by the parameters a, b, c.

In Figure 3, the plot corresponds to one fuzzy variable, with the x-axis indicating the crisp domain $x_i \in U_{x_i}$ and $y_j \in U_{y_j}$, and the y-axis representing the degree of membership $\mu(x) \in [0, 1]$. A detailed list of membership function parameters for each fuzzy term is provided in Table 2, specifying the triangular support points $[a, b, c]$ used in defining the fuzzification for both input and output variables. Figure 3 provides a detailed example of the fuzzification process applied to the input variable x_1 (road crack severity). In the case when a crisp input value $x = 7$ is received, it falls within the overlapping support ranges of the fuzzy sets *Medium* and *High*, defined by TriMFs with parameters $[a, b, c] = [2, 5, 8]$ and $[6, 10, 10]$, respectively. The system evaluates its degree of membership using Equation (12), as follows:

- **For Medium:** since $7 > b = 5$, then $\mu_{\text{Medium}}(7) = \dfrac{8-7}{8-5} = \dfrac{1}{3} \approx 0.33$.
- **For High:** since $7 < b = 10$, then $\mu_{\text{High}}(7) = \dfrac{7-6}{10-6} = \dfrac{1}{4} = 0.25$.

- **For Low:** since $x = 7$ is outside the triangle $[0, 0, 4]$, then $\mu_{\text{Low}}(7) = 0$.

The above scenario illustrates that the input is simultaneously classified as approximately 33% medium and 25% high, which shows partial membership in both categories. This approach of overlapping classification captures the uncertainty and gradual transitions often found in real-world conditions. These membership degrees are not just numeric scores but semantic indicators, thereby enabling the system to approximate human-like reasoning and to support robust decision-making in ambiguous or safety-critical environments. For comparison, Figure 4a (a) and Figure 4b (b) illustrate the same fuzzification process using Gaussian and trapezoidal membership functions. For a crack severity of 7, the Gaussian function yields partial memberships of approximately Medium = 0.42 and High = 0.58, while the trapezoidal function results in Medium = 0.5 and High = 0.7. Although both alternatives provide smoother or plateau-based representations, they require additional computation and may obscure the semantic clarity of rule boundaries. By contrast, triangular membership functions produce linear, transparent mappings that are more directly interpretable by decision-makers. Given that preliminary tests showed minimal differences in classification accuracy ($\leq$1%) across the three types, TriMFs were selected as the most practical trade-off for the proposed system.

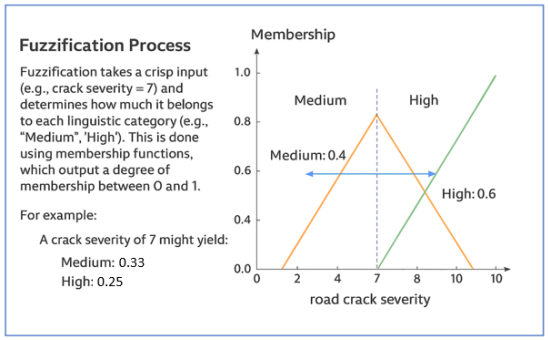

Figure 3: Illustration of the fuzzification process for the input variable *road crack severity*:

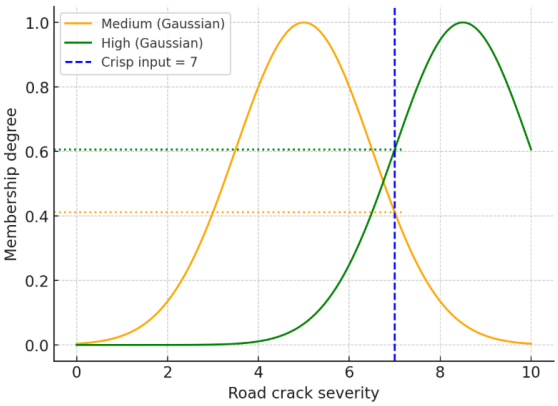

(a) Gaussian fuzzification

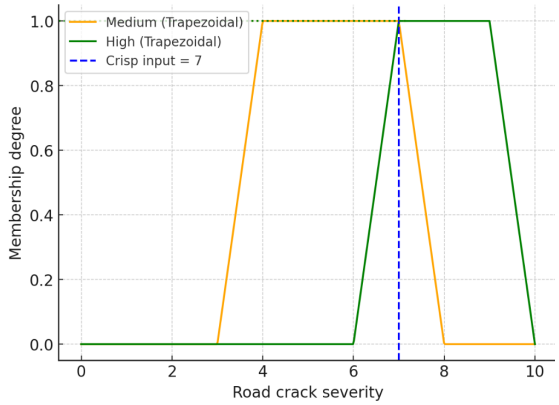

(b) Trapezoidal fuzzification

Figure 4: Alternative fuzzification functions for the input variable.

3.4.5 Rule base and inference engine

The fuzzy inference engine operates over a rule base R constructed from the combinations of linguistic input conditions and their corresponding output decisions. Each rule is expressed in the standard Mamdani IF–THEN form, which models the relationship between risk-contributing factors and the resulting pedestrian fall risk. A generic fuzzy rule R^r can be expressed as Equ (13)

$$R^r : \text{IF } x_1 \text{ is } A_1^{(r)} \text{ AND } x_2 \text{ is } A_2^{(r)} \text{ AND } x_3 \text{ is } A_3^{(r)} \text{ AND } x_4 \text{ is } A_4^{(r)} \Rightarrow y_1 \text{ is } B_1^{(r)},\ y_2 \text{ is } B_2^{(r)}, \tag{13}$$

where $A_i^{(r)} \in F_{x_i}$ are the fuzzy antecedents for input variable x_i, $B_j^{(r)} \in F_{y_j}$ are the fuzzy consequents for output y_j, and $r = \{1, 2, \cdots, R\}$ indexes the total rules in the rule base. In the proposed fuzzy scheme, each rule R^r is activated

by evaluating the degrees of membership obtained from the fuzzification module, and the rule firing strength $\alpha^{(r)}$ is computed using T-norm as Equation (14)

$$\alpha^{(r)} = \min\left\{\mu_{A_1^{(r)}}(x_1), \mu_{A_2^{(r)}}(x_2), \mu_{A_3^{(r)}}(x_3), \mu_{A_4^{(r)}}(x_4)\right\}. \tag{14}$$

For each fired rule, the consequent fuzzy sets $B_j^{(r)}$ are implicated using the Mamdani-style given in Equ (15) such that:

$$\mu_{B_j^{(r)}}(y_j) = \min\left(\alpha^{(r)}, \mu_{B_j}(y_j)\right). \tag{15}$$

This process generates clipped fuzzy outputs, which are aggregated across all R rules using the maximum operator such that:

$$\mu_{B_j^{(\text{agg})}}(y_j) = \max_r\left\{\mu_{B_j^{(r)}}(y_j)\right\}. \tag{16}$$

The total rule base in this study consists of $R = 54$ rules, developed through a three-step process:

1. **Literature-driven risk factors** – Candidate rules were first drafted from prior work on pedestrian fall risk, human factors, and pavement safety. For example, studies consistently highlight elderly pedestrians, wet/slippery surfaces, and poor visibility as key predictors of falls.
2. **Expert elicitation** – Three domain experts (two traffic engineers with >10 years' field experience, and one researcher in computational intelligence) refined these candidate rules. Selection criteria for experts included professional experience in road safety projects and academic contributions to intelligent transportation systems.
3. **Scenario-based reasoning** – Rules were stress-tested against real-world analogies. For example: IF severity = High, weather = Foggy, road = Slippery, and age = Elderly $\Rightarrow$ risk is **Very High**, fall rate $\approx 80\%$. This aligns with both theory and observed accident trends.

To formalize rule strength, a heuristic Risk Score S_r was computed for each rule as given in Equ (17):

$$S^{(r)} = \sum_{i=1}^{4} w_i \cdot \lambda_i(L_i^{(r)}). \tag{17}$$

Where, $L_i^{(r)}$ is the linguistic term assigned to the i^{th} antecedent of rule r, $\lambda_i : L_i \to \{1, 2, 3\}$ maps linguistic terms to ordinal severity levels, and $w_i \in [0, 1]$ is the importance weight of input x_i. These weights are driven by both expert elicitation and prior safety studies. For instance, *Age* received a higher weight due to strong evidence linking frailty to fall susceptibility, while *Weather (Foggy)* was weighted higher than *Clear* due to visibility loss. Example rules:

- IF Crack = High, Weather = Foggy, Road = Slippery, Age = Elderly $\Rightarrow$ Risk = Very High, Fall Rate = 80% (Score = 12).
- IF Crack = Low, Weather = Clear, Road = Dry, Age = Child $\Rightarrow$ Risk = Very Low, Fall Rate = 1% (Score = 5).

A subset of the 54 rules is listed in Table 3. To further examine the robustness of these heuristic assignments, a sensitivity analysis was performed (Fig. 5a). Perturbing each input weight by $\pm 20\%$ showed that *Age* produced the largest label shifts, followed by *Weather* and *Road*, confirming its dominant role in risk assessment. Figure 5a presents the sensitivity of fuzzy rule outputs under $\pm 20\%$ perturbation of input weights, where *Age* produced the largest variations in assigned labels, followed by *Weather* and *Road*, confirming its influence in risk assessment. In addition, a logistic regression sanity-check trained on the synthetic scenario dataset (Fig. 5b) identified *Elderly*, *Slippery roads*, and *Foggy weather* as the strongest predictors of high fall risk. This analysis was carried out for predicting High/Very High fall risk from synthetic scenarios. The findings support the heuristic weight assignments in the rule base.

The above analysis (Figs. 5) is conducted to support the heuristic weight design while retaining transparency and interpretability. Although this rule base demonstrates consistency with expected safety-critical patterns, it is acknowledged that it remains heuristic. In future work, the weights and rules can be empirically calibrated using larger annotated datasets and further enhanced through hybrid fuzzy learning approaches. This will enable adaptive updating of the rule base, improve scalability, and benchmark performance against more advanced fuzzy frameworks.

Table 3 presents a representative subset of the 54 fuzzy rules used for pedestrian fall risk estimation, each encoded with a unique combination of antecedent terms and the corresponding output decisions (Fall Risk Level, Fall Rate), along with their heuristic risk score $S^{(r)}$.

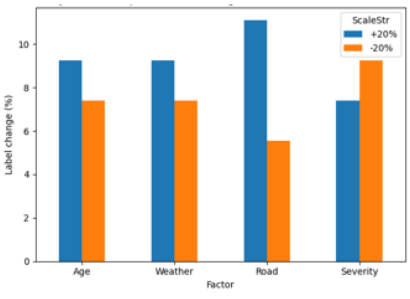

(a) Sensitivity of rule outputs to ±20% weight perturbations

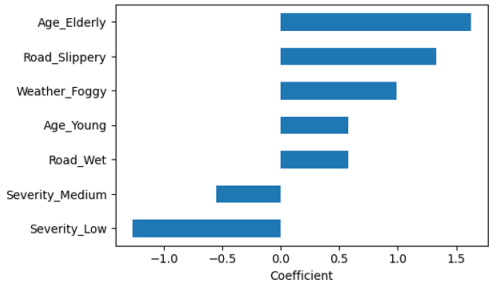

(b) Logistic regression coefficients highlighting key fall-risk predictors

Figure 5: Analysis of model robustness and interpretability: (a) sensitivity of rule outputs under weight perturbations, (b) logistic regression coefficients for fall-risk predictors.

Table 3: Sample visualization of the Fuzzy Rules for Pedestrian Fall Risk Estimation

Crack Severity	**Weather**	**Road**	**Pedestrian Age**	**Risk Level**	**Fall Rate**	**Score**
High	Foggy	Slippery	Elderly	Very High	80.00%	12
Low	Clear	Wet	Young	Very Low	1.00%	5
Medium	Foggy	Wet	Elderly	Very High	80.00%	10
Low	Clear	Dry	Elderly	Low	5.00%	6
High	Clear	Dry	Young	Low	5.00%	6
Medium	Foggy	Dry	Elderly	High	50.00%	9
High	Clear	Wet	Child	Medium	20.00%	8
Low	Clear	Dry	Child	Very Low	1.00%	5
Medium	Foggy	Wet	Young	Medium	20.00%	8
High	Foggy	Slippery	Child	Very High	80.00%	11
Medium	Foggy	Slippery	Young	High	50.00%	9
Low	Clear	Wet	Elderly	Low	5.00%	7
...						

3.4.6 Defuzzification and output interpretation

In this final stage of the proposed FIS, the aggregated fuzzy outputs for each variable $y_j \in \{y_1, y_2\}$ are converted to crisp values via defuzzification operation[31]. Here, y_1 represents the Fall Risk Level (a qualitative output expressed in *Very Low* $\rightarrow$ *Very High* categories), whereas y_2 denotes the Fall Rate (a quantitative probability estimate, e.g., 1% $\rightarrow$ 80%). This distinction avoids ambiguity and ensures that the two outputs provide complementary but non-redundant information. The proposed system adopts the centroid method due to its robustness, continuity, and semantic interpretability [21].

The computation of the crisp output y_j^* is given in Equ (18):

$$y_j^* = \frac{\int_{\mathcal{U}_{y_j}} y_j \cdot \mu_{B_j^{(\text{agg})}}(y_j)\, dy_j}{\int_{\mathcal{U}_{y_j}} \mu_{B_j^{(\text{agg})}}(y_j)\, dy_j}. \tag{18}$$

Where, $\mu_{B_j^{(\text{agg})}}(y_j)$ denotes the aggregated membership function of all fired rules for output y_j, $\mathcal{U}_{y_j}$ is the universe of discourse for y_j, and $y_j^* \in [0, 100]$ is the defuzzified crisp value which represents the output i.e., estimated Fall Risk Level (y_1) or Fall Rate (y_2).

To facilitate human-centric interpretation, the system then identifies the closest linguistic label $\tilde{B}_j \in F_{y_j}$ corresponding to the highest degree of membership at y_j^*:

$$\tilde{B}_j = \arg\max_{B \in F_{y_j}} \mu_B(y_j^*). \tag{19}$$

The above Equation (19) computes the centroid (center of gravity) of the aggregated fuzzy output set, which provides

a representative crisp value that balances all activated rules proportionally to their firing strengths. This means the system produces a smooth and interpretable output even under partial or conflicting input conditions.

For example, when a young pedestrian walks on a slightly cracked but slippery road in foggy weather, the fuzzy rule base can simultaneously activate low-risk and high-risk rules with different impact intensities. Instead of making abrupt or binary decisions, the centroid approach collapses all these activations into a single representative risk level, retaining the nuances of uncertainty and helping to make better, situation-aware decisions.

The proposed pedestrian fall risk assessment framework is designed for high-traffic areas such as urban sidewalks, transportation hubs, and public parks, where variable pavement conditions and environmental factors may increase the risk of falls. By combining human-centered reasoning with multi-factor risk assessment, the system enables decision support for proactive safety intervention, resource prioritization, and smart city infrastructure planning.

4 Result and outcome analysis

This section presents the experimental results and evaluates the performance of the proposed integrated framework for road crack severity assessment and pedestrian fall risk analysis. The evaluation is performed in three phases: (i) crack width quantification, (ii) crack severity classification, and (iii) FIS-based pedestrian fall risk evaluation. All experiments were implemented in Python 3.9 under Anaconda on a 64-bit Windows 11 system. Performance evaluation includes both qualitative and quantitative analysis. Qualitative assessment involves visual inspection of crack maps, confusion matrices, activation maps, and graphical analyses. Quantitative evaluation uses standard metrics: accuracy, precision, recall, F1-score, mean absolute error (MAE), root mean square error (RMSE), and Pearson correlation coefficient (R). MAE and RMSE are applied to crack width evaluation, defined as follows:

$$\text{MAE} = \frac{1}{n}\sum_{i=1}^{n}|y_i - \hat{y}_i|, \quad \text{RMSE} = \sqrt{\frac{1}{n}\sum_{i=1}^{n}(y_i - \hat{y}_i)^2},$$

y_i denotes the ground truth data and $\hat{y}_i$ is the predicted data. The classification performance metrics are:

$$\text{Accuracy} = \frac{TP+TN}{TP+TN+FP+FN}, \quad \text{Precision} = \frac{TP}{TP+FP}, \quad \text{Recall} = \frac{TP}{TP+FN}, \quad F1_{\text{Score}} = 2 \times \frac{\text{Precision} \times \text{Recall}}{\text{Precision} + \text{Recall}}.$$

4.1 Validation of the proposed crack quantification method

Due to the lack of direct ground truth for crack width in public datasets, validation was conducted via a transparent comparison using a small, manually annotated test set of 60 images. Human annotators marked the visually-identified maximum width for each crack segment. The proposed adaptive segmentation and distance-based width computation were evaluated against these manual ground-truth (GT) measurements and the standard skeleton-based Euclidean distance transform (EDT) method [17]. For each method, maximum width and location were compared using MAE, RMSE, and Pearson correlation coefficient (R).

Figure 6 shows regression plot analysis for the proposed automated crack width versus manual ground truth. It can be seen that most computed widths closely cluster around the identity line, indicating strong agreement with manual annotation. Although a few outliers are present, the overall trend demonstrates minimal bias and high reliability.

Table 4 compares the proposed crack quantification scheme with the standard EDT method. The proposed method achieves the lowest MAE (4.46 pixels) and RMSE (5.82 pixels), thereby outperforming the standard EDT, which shows higher error rates and lower correlation. The high R value of 0.98 indicates a strong positive linear relationship between predicted and manually annotated widths. Overall, the results demonstrate the effectiveness and reliability of the proposed method across various crack geometries. Figure 7 presents a histogram analysis showing that the proposed segmentation-based width computation consistently produces low errors for most test images, confirming its reliability and precision. The narrow peak at low error values reflects minimal deviation from manual annotation, especially for thin cracks. In contrast, the simple EDT approach, lacking segmentation and intersection handling, shows higher error variability and less robustness on irregular or branched cracks. The proposed method effectively addresses these issues and remains accurate even when local linearity or continuity assumptions fail.

4.2 Validation of crack severity prediction model

Due to the absence of public datasets with severity labels, model validation used a custom-annotated crack image dataset. Comparative analysis with baseline CNN architectures demonstrated performance improvements, while test-

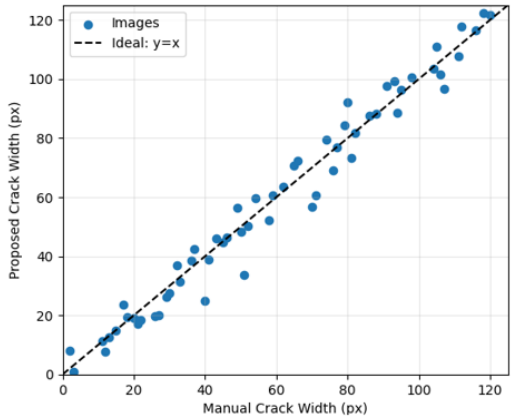

Figure 6: Regression plot analysis of automated crack width estimation versus manual ground truth.

Table 4: Performance comparison between the proposed crack quantification scheme and the standard EDT method.

Metrics	Simple EDT	Proposed
MAE	11.25	4.46
RMSE	24.87	5.82
R (Pearson)	0.954	0.986
Min Error	0.01	0.10
Max Error	61.3	58.9

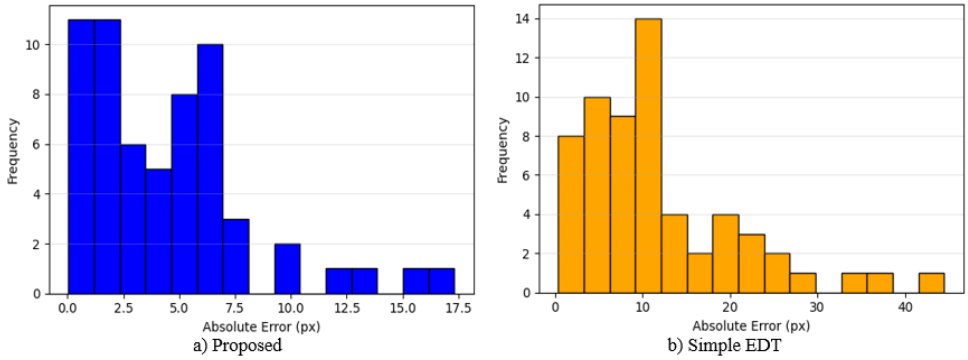

Figure 7: Analysis of the absolute error distribution

ing on transformed images (simulating noise, brightness variations, and blur) assessed robustness and real-world applicability. Grad-CAM visualizations were also used to interpret model decisions and confirm that severity predictions relied on relevant crack features. VGG16 and EfficientNetB0 reached the highest accuracy, but EfficientNetB0 was selected as the main model due to its competitive accuracy and lightweight architecture compared to the more complex VGG16. The confusion matrix shown in Figure 8a shows the model's correct and incorrect predictions for each crack severity class, with an overall test accuracy of 95%. For the high severity class, 166 out of 173 images were correctly classified, with only seven misclassified. In the low severity class, 229 to 239 instances were accurately predicted, and 10 were misclassified as medium. The medium severity class showed slightly more misclassifications, with 268 out of 295 correctly classified. The confusion matrix demonstrates the model's ability to distinguish between severity levels, with only minor errors.

Figure 8b presents the ROC curves, illustrating the model's discriminative capability. The high AUC values (ranging from 0.97 to 1.00) for all classes indicate that the model is highly effective at classifying crack severity, particularly for the no crack, low, and medium severity categories. These results demonstrate strong generalization to unseen data, with a good balance between true positives and false positives across thresholds. The Table 5 shows the classification performance in terms of precision, recall, and F1-score. The model achieved strong results across all severity classes. Notably, the *no_crack* class reached perfect precision, recall, and F1-score (100%), demonstrating excellent non-damaged surfaces detection. For the high severity class, the F1-score was 96%, with both precision and recall at 96%. The low and medium severity classes also had high F1-scores of 95% and 94%, respectively. These results indicate that the model effectively distinguishes between different crack severity levels, with minimal misclassification.

Figure 9a displays Grad-CAM activation maps for low, medium, and high severity classes. The highlighted regions closely correspond to the actual crack structures, with the model focusing on wider cracks in high-severity cases and thin, isolated cracks in low-severity severity. This demonstrates that the model accurately localizes and differentiates

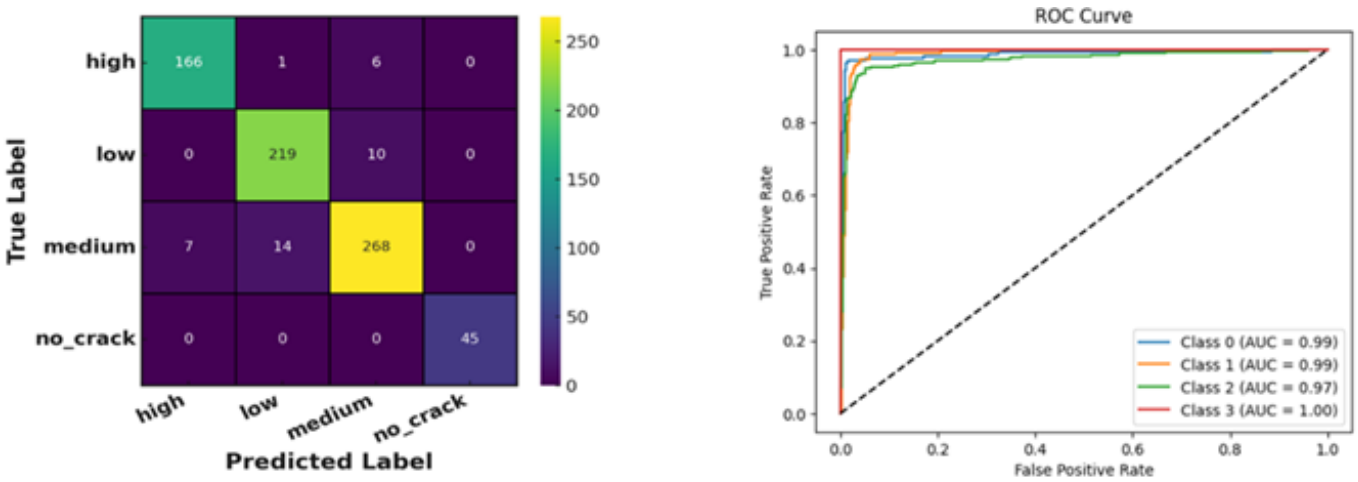

(a) Confusion matrix for trained model on test dataset (b) ROC plot for trained model on test dataset

Figure 8: Performance evaluation of the trained model on the test dataset: (a) confusion matrix, (b) ROC curve.

Table 5: Outcome analysis of precision, recall, and F1-score for crack severity classes

Class	Precision	Recall	F1-Score
High	96%	96%	96%
Low	94%	96%	95%
Medium	94%	93%	94%
No_Crack	100%	100%	100%

cracks based on width, supporting its reliability and transparency in severity assessment. These explainability results confirm that predictions are driven by physically relevant features, increasing trust in the model.

Figure 9b shows the model's performance on crack images with simulated noise, low lighting, and blur. For all severity classes, the model maintained high prediction confidence and correct classifications, even under harsh conditions. These results indicate strong robustness and generalization to data quality variability, making the model suitable for real-world deployment with diverse sensor and environmental conditions.

4.3 Validation of the fuzzy-based pedestrian fall risk

The proposed fuzzy inference-based pedestrian fall risk model was evaluated using a dataset of 3,240 dynamic scenarios generated through a combinatorial approach, covering all environmental and demographic configurations with expert-driven rules. The FIS was benchmarked against three non-fuzzy methods: (i) CRISP thresholding,(ii) a multilayer perceptron (MLP) with two hidden layers (64 and 32 neurons), and (iii) a support vector machine (SVM) with RBF kernel and tuned via 5-fold cross-validation. 70% of the data was used for training MLP and SVM, with the remaining 972 samples for evaluation. Table 6 shows that the proposed FIS outperformed all baselines, achieving 95% (±1%) accuracy and 92% (±2%) F1-score. The FIS also achieved a lower MAE of 3.3 (±0.6), compared to higher MAE values for CRISP, MLP, and SVM, demonstrating its superior ability to handle complex interactions between input variables. The proposed FIS was also evaluated for processing time, achieving a response time of 2100 ms—slightly higher than CRISP but faster than MLP and SVM, demonstrating an effective balance between speed and accuracy for real-time deployment. Paired t-test analysis further confirmed the statistical significance of FIS performance, with p-values of 0.004 and 0.006 against MLP and SVM, respectively, at a 95% confidence level, indicating reduced misclassification of high-risk scenarios.

Additionally, ablation analysis was performed by removing each input variable to assess its impact on accuracy, as shown in Table 7, which shows that the whole model configuration achieved the highest accuracy across all methods, with FIS at 95%, followed by MLP (88%), SVM (86%), and CRISP (79%). Removing each input variable led to performance drops for all models, but FIS showed higher resilience; for example, eliminating pedestrian age reduced FIS accuracy by 17.9% (vs. 22.8% for CRISP), highlighting its robustness with partial inputs. Road condition and weather had a milder impact on FIS than non-fuzzy models, underscoring the model's multidimensional interpretability.

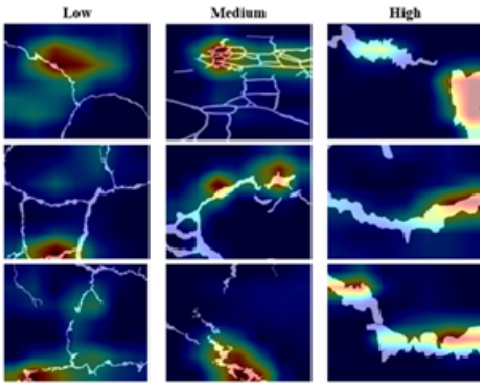

(a) Activation-based explainability

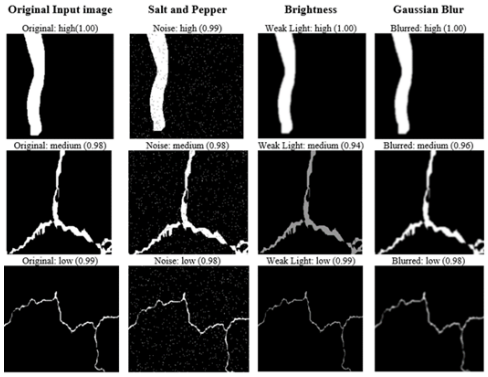

(b) Robustness analysis under environment variability

Figure 9: Illustration of model evaluation: (a) activation-based explainability, (b) robustness analysis under environment variability.

The following assessment regarding sensitivity analysis, as shown in Figure 10, assessed robustness to noisy inputs by adding Gaussian noise (0–40%). FIS exhibited only a 0.5-unit increase in MAE, compared to higher increases for MLP (1.8), SVM (1.4), and CRISP (2.6). Failure count analysis confirmed that FIS maintained fewer misclassifications under perturbation, especially in high-risk categories where accurate prediction is essential. On the other hand, the Panel C in Figure 10 depicts the F1-score trend under increasing noise, whereas all models show gradual performance drop-offs. Still, FIS maintains a relatively flat slope, retaining an F1-score above 0.8 even at 40% noise, whereas CRISP drops below 0.6. The above outcome analysis indicates that the proposed FIS offers stronger noise tolerance with higher predictive reliability under partial and imprecise data conditions, essential for real-world deployment scenarios.

Table 8 presents a qualitative comparative analysis of the proposed FIS against non-fuzzy baseline approaches. The proposed FIS exhibits the highest accuracy and offers clear interpretability through rule-based reasoning, an essential aspect in safety-critical domains such as pedestrian risk assessment. On the other hand, MLP and SVM suffer from low transparency due to their black-box nature. In terms of robustness to noise, FIS demonstrates strong tolerance, as supported by the prior sensitivity analysis. The processing time for FIS is slightly higher than CRISP but significantly lower than the data-driven models, MLP and SVM, thereby achieving a balance between responsiveness and decision quality. The training-free nature of FIS enhances its deployability, especially in contexts with limited data availability. Furthermore, the system design of the FIS allows for high scalability and adaptability, enabling rule updates or extensions without retraining, which is also essential for real-time deployment.

Table 6: Comparative performance evaluation

Model	**Accuracy ↑**	**F1-Score ↑**	**MAE ↓**	**Processing Time (ms) ↓**	**p-value (vs. FIS)**
CRISP	79% (0.03)	75% (0.04)	10.2 (1.1)	1400	$< 1e^{-3}$
MLP	88% (0.02)	85% (0.03)	6.1 (0.9)	5700	0.004
SVM	86% (0.02)	85% (0.02)	6.6 (1.0)	4300	0.006
Proposed FIS	95% (0.01)	92% (0.02)	3.3 (0.6)	2100	—

Table 7: Ablation analysis

Removed Input Variable	**FIS Accuracy ↓**	**Δ FIS**	**MLP Accuracy ↓**	**Δ MLP**	**SVM Accuracy ↓**	**Δ SVM**	**CRISP Accuracy ↓**	**Δ CRISP**
None	0.95	—	0.88	—	0.86	—	0.79	—
Pedestrian Age	0.78	−17.9%	0.72	−18.2%	0.67	−22.1%	0.61	−22.8%
Road Condition	0.83	−12.6%	0.77	−12.5%	0.72	−16.3%	0.65	−17.7%
Weather Condition	0.87	−8.4%	0.81	−8.0%	0.76	−11.6%	0.71	−10.1%
Crack Severity	0.90	−5.3%	0.84	−4.5%	0.79	−8.1%	0.75	−5.1%

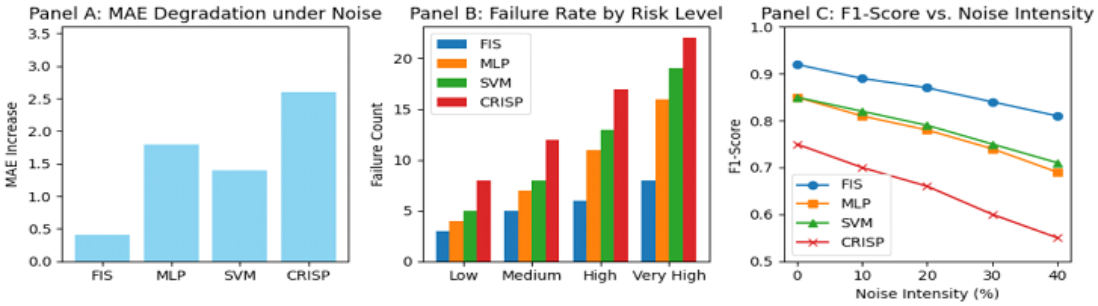

Figure 10: Sensitivity analysis

Table 8: Qualitative comparative analysis of the proposed FIS vs. Non-Fuzzy models

Criteria	Proposed FIS	CRISP	MLP	SVM
Accuracy	95%	78%	87%	84%
Interpretability	High (Rule-based)	Moderate	Low (Black-box)	Low
Robustness to Noise	High (Tolerant)	Low	Moderate	Moderate
Processing Time	2.1 sec	1.4 sec	5.7 sec	4.3 sec
Complexity	Moderate	Low	High	Moderate
Scalability	High (Modular rules)	Low	High	Moderate
Training Required	No (Expert rules)	No	Yes (Large data)	Yes
Transparency	High (Linguistic)	Moderate	Low	Low
Adaptability	High (Rule updates)	Low	Moderate	Moderate

4.4 Limitation

The proposed system demonstrates robust and accurate crack width quantification using 2D imagery, but there are some limitations and scope as discussed below:

- The current research considers crack width measurements extracted from 2D surface images and does not capture vertical displacement, depth, or subsurface features of cracks, which are crucial for a comprehensive assessment of structural severity and pavement integrity. In practice, the severity of cracks is often a combination of both surface width and depth; for example, narrow but deep cracks can pose greater risks to structural stability than wide but shallow ones.
- Although 2D pixel-width remains a practical and widely-used proxy for severity in the absence of 3D data, there is no standard or benchmarked dataset available that consists of 3D road crack images. Future extensions of this work will therefore explore integration with 3D reconstruction techniques such as stereo vision, LiDAR scanning, photogrammetry, and structured-light sensors, which can provide depth maps and geometric profiles of pavement cracks. These approaches would allow for more comprehensive indicators of crack severity, including depth, slope, and volume, which cannot be inferred from 2D imagery alone.
- The absence of publicly available, annotated datasets with ground truth crack depth and severity metrics further restricts the comparison of this study with other works in the literature. Developing or contributing to benchmark datasets that combine both 2D and 3D crack annotations will be a priority for future research, as such datasets would enable more rigorous evaluation and facilitate fair comparisons across methods.

5 Conclusion

This paper presented an integrated system using image processing, machine learning, and fuzzy logic to automate road crack detection, severity classification, and pedestrian fall risk assessment. The system extracted crack metrics and used CNNs for classification, though class imbalance affected precision and recall. A fuzzy logic framework combined environmental factors and demographics for real-time risk assessment. The experimental outcomes show the effectiveness of the proposed work, and the results were found to be promising for each module of the proposed framework.

The proposed system has direct practical implications by enabling automated crack quantification and severity assessment. It can support urban authorities in prioritizing maintenance of sidewalks and pedestrian walkways, par-

ticularly in high-density Indian cities where manual inspection is still prevalent. The fuzzy inference model further provides interpretable fall risk levels, which can assist safety regulators and smart city planners in making proactive interventions such as targeted repairs, improved signage, or restricted access in hazardous areas. Importantly, the system's interpretable design makes it suitable for integration into decision-support tools for municipal agencies, bridging the gap between technical crack analysis and public safety management.

In future work, the study will focus on addressing current limitations to improve the robustness of the fuzzy-based system by incorporating additional contextual factors such as traffic density, pedestrian flow, and route familiarity. Another important direction will be the integration of vertical displacement analysis using stereo imaging or LiDAR sensors, which can substantially refine severity assessments beyond width-based classification, but is challenging due to the absence of available standardized datasets providing crack depth quantification. The development of benchmark datasets combining both 2D and 3D crack attributes will also be a priority, enabling fairer comparisons across approaches and strengthening the system's applicability in real-world deployments.

References

[1] L. Ali, H. Al-Jassmi, M. Swavaf, W. Khan, F. Alnajjar, *RS-Net: Residual sharp u-net architecture for pavement crack segmentation and severity assessment*, Journal of Big Data, **11**(1) (2024), 116. https://doi.org/10.1186/s40537-024-00981-y

[2] A. Ali, U. Heneash, A. Hussein, M. Eskebi, *Predicting pavement condition index using fuzzy logic technique*, Infrastructures, **7**(7) (2022), 91. https://doi.org/10.3390/infrastructures7070091

[3] M. Bhardwaj, N. U. Khan, V. Baghel, *Road crack detection using pixel classification and intensity-based distinctive fuzzy c-means clustering*, Visual Computer, **41** (2025), 1689-1704. https://doi.org/10.1007/s00371-024-03470-8

[4] P. S. Chakurkar, D. Vora, S. Patil, K. Kotecha, *Automated crack localization for road safety using contextual u-net with spatial-channel feature integration*, MethodsX, **13** (2024), 102796. https://doi.org/10.1016/j.mex.2024.102796

[5] F. Demir, E. Yalcin, M. Yilmaz, *CrackNet: A new deep learning-based strategy for automatic classification of road cracks after earthquakes*, Engineering Science and Technology, an International Journal, **69** (2025), 102128. https://doi.org/10.1016/j.jestch.2025.102128

[6] L. Deng, A. Zhang, J. Guo, Y. Liu, *An integrated method for road crack segmentation and surface feature quantification under complex backgrounds*, Remote Sensing, **15**(6) (2023), 1530. https://doi.org/10.3390/rs15061530

[7] F. Elghaish, S. Matarneh, E. Abdellatef, F. Rahimian, M. R. Hosseini, A. F. Kineber, *Multi-layers deep learning model with feature selection for automated detection and classification of highway pavement cracks*, Smart and Sustainable Built Environment, **14**(2) (2025), 511-535. https://doi.org/10.1108/SASBE-09-2023-0251

[8] A. Galanis, G. Botzoris, N. Eliou, *Pedestrian road safety in relation to urban road type and traffic flow*, Transportation Research Procedia, **24** (2017), 220-227. https://doi.org/10.1016/j.trpro.2017.05.111

[9] H. Gong, L. Liu, H. Liang, Y. Zhou, L. Cong, *A state-of-the-art survey of deep learning models for automated pavement crack segmentation*, International Journal of Transportation Science and Technology, **13** (2024), 44-57. https://doi.org/10.1016/j.ijtst.2023.11.005

[10] J. Ha, D. Kim, M. Kim, *Assessing severity of road cracks using deep learning-based segmentation and detection*, Journal of Supercomputing, **78**(16) (2022), 17721-17735. https://doi.org/10.1007/s11227-022-04560-x

[11] N. D. Hoang, Q. L. Nguyen, *Automatic recognition of asphalt pavement cracks based on image processing and machine learning approaches: A comparative study on classifier performance*, Mathematical Problems in Engineering, **2018** (2018), 1-16. https://doi.org/10.1155/2018/6290498

[12] I. Hussain, L. Alam, *Adaptive road crack detection and segmentation using Einstein operators and ANFIS for real-time applications*, Journal of Intelligent Systems and Control, **3**(4) (2024), 213-226. https://doi.org/10.56578/jisc030402

[13] D. A. Jehu, J. C. Davis, R. S. Falck, K. J. Bennett, D. Tai, M. F. Souza, B. R. Cavalcante, M. Zhao, T. Liu-Ambrose, *Risk factors for recurrent falls in older adults: A systematic review with meta-analysis*, Maturitas, **144** (2021), 23-28. https://doi.org/10.1016/j.maturitas.2020.10.021

[14] M. Karaşahin, S. Terzi, *Performance model for asphalt concrete pavement based on the fuzzy logic approach*, Transport, **29**(1) (2014), 18-27. https://doi.org/10.3846/16484142.2014.893926

[15] R. Kumar, S. Tung, *Automated detection and severity assessment of asphalt pavement distress using YOLOv8: A deep learning approach*, International Journal of Pavement Research and Technology, (2025). https://doi.org/10.1007/s42947-025-00584-7

[16] C. Liu, C. S. Tang, B. Shi, W. B. Suo, *Automatic quantification of crack patterns by image processing*, Computational and Geosciences, **57** (2013), 77-80. https://doi.org/10.1016/j.cageo.2013.04.008

[17] W. Liu, C. Zhang, H. Ma, Y. Li, *Distance transform-based skeleton extraction and its applications in sensor networks*, IEEE Transactions on Parallel and Distributed Systems, **24**(9) (2013), 1763-1772. https://doi.org/10.1109/TPDS.2012.300

[18] S. Mathavan, V. Kanapathippillai, A. Kumar, C. Chandrakumar, K. Kamal, M. Rahman, M. Stonecliffe-Jones, *Detection of pavement cracks using tiled fuzzy Hough transform*, Journal of Electronic Imaging, **26**(5) (2017). https://doi.org/10.1117/1.JEI.26.5.053008

[19] H. Oliveira, P. L. Correia, *Automatic road crack detection and characterization*, IEEE Transactions on Intelligent Transportation Systems, **14**(1) (2013), 155-168. https://doi.org/10.1109/TITS.2012.2208630

[20] S. Qiu, W. Wang, S. Wang, K. C. P. Wang, *Methodology for accurate AASHTO PP67-10-based cracking quantification using 1-mm 3D pavement images*, Journal of Computing in Civil Engineering, **31**(2) (2017), 04016056. https://doi.org/10.1061/(ASCE)CP.1943-5487.0000627

[21] N. M. Ralevic, M. Delic, L. Nedovic, *Aggregation of fuzzy metrics and its application in image segmentation*, Iranian Journal of Fuzzy Systems, **19**(3) (2022), 19-37. https://doi.org/10.22111/ijfs.2022.6941

[22] S. Ranjbar, F. Moghadas Nejad, H. Zakeri, *Image-based severity analysis of asphalt pavement bleeding using a metaheuristic-boosted fuzzy classifier*, Automation in Construction, **166** (2024), 105655. https://doi.org/10.1016/j.autcon.2024.105655

[23] A. G. Rundle, R. P. Crowe, H. E. Wang, A. X. Lo, *A methodology for the public health surveillance and epidemiologic analysis of outdoor falls that require an emergency medical services response*, Injury Epidemiology, **10**(1) (2023), 4. https://doi.org/10.1186/s40621-023-00414-z

[24] F. Saeed, M. Rahman, M. Mahmood, *A fuzzy inference system for predicting pavement surface damage due to combined action of traffic loading and water*, International Journal of Pavement Engineering, **23**(2) (2020), 261-269. https://doi.org/10.1080/10298436.2020.1742333

[25] W. Song, G. Jia, D. Jia, H. Zhu, *Automatic pavement crack detection and classification using multiscale feature attention network*, IEEE Access, **7** (2019), 171001-171012. https://doi.org/10.1109/ACCESS.2019.2956191

[26] J. Swanenburg, E. D. de Bruin, D. Uebelhart, T. Mulder, *Falls prediction in elderly people: A 1-year prospective study*, Gait and Posture, **31**(3) (2010), 317-321. https://doi.org/10.1016/j.gaitpost.2009.11.013

[27] L. Wang, Q. Feng, J. Yan, *Pavement crack detection based on depth-supervision FRRN model*, Measurement and Control, **58**(8) (2024), 1078-1088. https://doi.org/10.1177/00202940241292189

[28] Q. Yang, Y. Deng, *Evaluation of cracking in asphalt pavement with stabilized base course based on statistical pattern recognition*, International Journal of Pavement Engineering, **20**(4) (2017), 417-424. https://doi.org/10.1080/10298436.2017.1299528

[29] X. Yang, H. Li, Y. Yu, X. Luo, T. Huang, X. Yang, *Automatic pixel-level crack detection and measurement using fully convolutional network*, Computer-Aided Civil and Infrastructure Engineering, **33**(12) (2018), 1090-1109. https://doi.org/10.1111/mice.12412

[30] M. Yilmaz, et al., *Automatic segmentation of asphalt cracks on highways after large-scale and severe earthquakes using deep learning-based approaches*, IEEE Access, **13** (2025), 22820-22830. https://doi.org/10.1109/ACCESS.2025.3536554

[31] J. Yuan, Q. Ren, C. Jia, J. Zhang, J. Fu, M. Li, *Automated pixel-level crack detection and quantification using deep convolutional neural networks for structural condition assessment*, Structures, **59** (2024), 105780. https://doi.org/10.1016/j.istruc.2023.105780